Communications

Fluorescent Probes

Y. Hori, K. Nakaki, M. Sato, S. Mizukami, K. Kikuchi* ——— ■■■■–■■■■

Development of Protein-Labeling Probes with a Redesigned Fluorogenic Switch Based on Intramolecular Association for No-wash Live-Cell Imaging

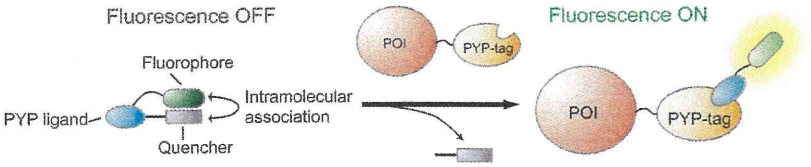

Turn on the switch: Fluorogenic probes for protein labeling based on the photoactive yellow protein (PYP) tag were developed. The fluorescence of the probes is turned off by intramolecular association and switched on by the reversal of this interaction upon reaction with the PYP tag that is fused to the protein of interest (POI, see scheme). The rapid and specific labeling reaction enabled the imaging of cell-surface proteins without washing.

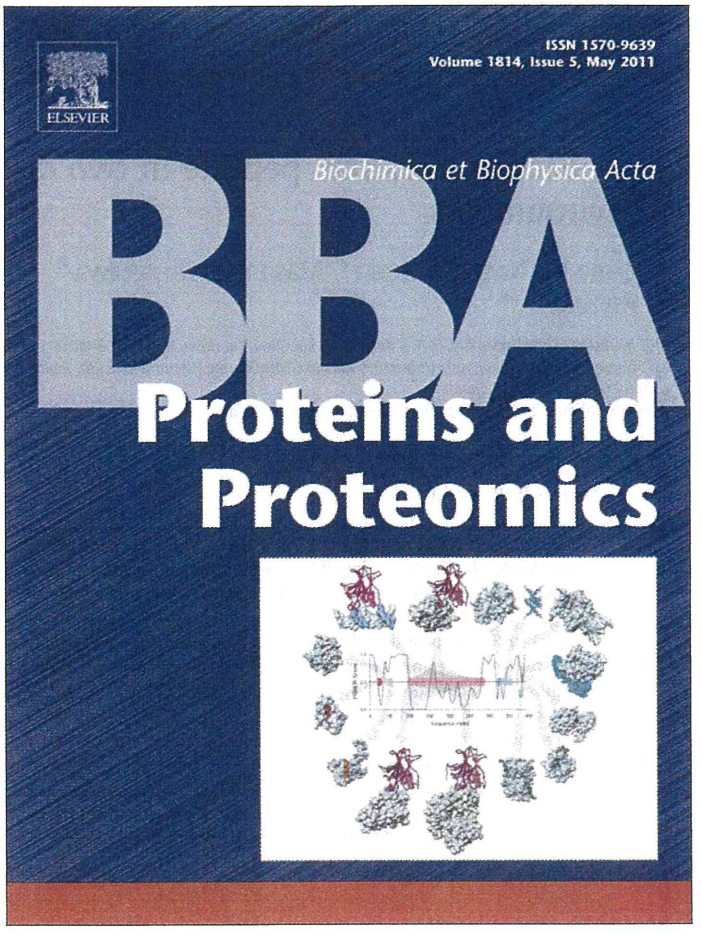

Biochimica et Biophysica Acta 1814 (2011) 724–730

Contents lists available at ScienceDirect

Biochimica et Biophysica Acta

journal homepage: www.elsevier.com/locate/bbapap

Structural difference of vasoactive intestinal peptide in two distinct membrane-mimicking environments

Yoshitaka Umetsu [a], Takeshi Tenno [a,b], Natsuko Goda [a], Masahiro Shirakawa [b], Takahisa Ikegami [c], Hidekazu Hiroaki [a,d,*]

[a] Division of Structural Biology, Graduate School of Medicine, Kobe University, 7-5-1 Kusunoki-cho, Chuo-ku, Kobe, Hyogo 650-0017, Japan
[b] Department of Molecular Engineering, Graduate School of Engineering, Kyoto University, Katsura, Nishikyo-ku, Kyoto 615-8530, Japan
[c] Institute of Protein Research, Osaka University, Suita, Osaka 565-0871, Japan
[d] Global Center of Excellence Program for Integrative Membrane Biology, Kobe University, Kobe, Hyogo, Japan

ARTICLE INFO

Article history:
Received 14 January 2011
Received in revised form 9 March 2011
Accepted 16 March 2011
Available online 23 March 2011

Keywords:
Vasoactive intestinal peptide
Pituitary adenylate cyclase-activating peptide
G protein-coupled receptor
NMR structure
Dodecylphosphocholine micelle

ABSTRACT

Vasoactive intestinal peptide (VIP) is a 28-amino acid neuropeptide which belongs to a glucagon/secretin superfamily, the ligand of class II G protein-coupled receptors. Knowledge for the conformation of VIP bound to membrane is important because the receptor activation is initiated by membrane binding of VIP. We have previously observed that VIP-G (glycine-extended VIP) is unstructured in solution, as evidenced by the limited NMR chemical shift dispersion. In this study, we determined the three-dimensional structures of VIP-G in two distinct membrane-mimicking environments. Although these are basically similar structures composed of a disordered N-terminal region and a long α-helix, micelle-bound VIP-G has a curved α-helix. The side chains of residues Phe[6], Tyr[10], Leu[13], and Met[17] found at the concave face form a hydrophobic patch in the micelle-bound state. The structural differences in two distinct membrane-mimicking environments show that the micelle-bound VIP-G localized at the water–micelle boundary with these side chains toward micelle interior. In micelle-bound PACAP-38 (one of the glucagon/secretin superfamily peptide) structure, the identical hydrophobic residues form the micelle-binding interface. This result suggests that these residues play an important role for the membrane binding of VIP and PACAP.

1. Introduction

Vasoactive intestinal peptide (VIP), a member of the glucagon/secretin superfamily, is a 28-amino acid neuropeptide that is evolutionarily well conserved from fish (cod) and frogs to humans. In mammals, except guinea pigs, the sequence identity is at least 85% [1]. VIP widely presents in the central and peripheral nervous systems. It acts in a wide range of physiological and pathological processes related to development, growth, and the control of neuronal and endocrine cells; it also functions in the digestive, respiratory, reproductive, and cardiovascular systems. Furthermore, VIP plays key roles in cancers, immune responses, and circadian rhythm [2]. It is a class II G protein-coupled receptor (GPCR) ligand that acts through interaction with two receptor subtypes (VPAC1 and VPAC2) [3]. VIP shares 68% homology with its closely related homolog, pituitary adenylate cyclase-activating polypeptide (PACAP), another secretin family member peptide [4,5], and both VIP and PACAP bind to VPAC1 and VPAC2 with equivalent affinities [6]. On binding of VIP to VPAC1 or VPAC2, the cyclic adenosine 5′-phosphate level increases significantly [7], while adenylate cyclase [8] and phospholipase C [9] are also activated, followed by divergent downstream effects through various transcription factors.

Recently, key biological functions of VPAC1 and VPAC2 in innate immune responses have emerged [10], and thus, the therapeutic potential of VIP agonists as well as VIP itself is promising [11]. The increased number of studies supporting the therapeutic potential of VIP includes the murine models of pancreatitis [12], human Crohn's disease (TNBS-induced colitis) [13,14], bacterial sepsis (survival model) [15], and human rheumatoid arthritis (RA; collagen-induced model) [16]. In the first example of the pancreatitis model, a selective VPAC1 agonist rather than VIP itself provides therapeutic benefits because of the opposing action of VPAC2 against VPAC1. In addition, in the other three cases (Crohn's disease, sepsis survival, and RA), the potential anti-inflammatory effect of VIP itself works well, most probably through suppression of inflammatory cytokines such as TNF-alpha and IL-6.

In addition to the therapeutic use of VIP, specific molecular interactions between VIP–VIP receptors are also useful in diagnosis

Abbreviations: NMR, nuclear magnetic resonance; TRX, thioredoxin; PACAP, pituitary adenylate cyclase-activating polypeptide; VIP, vasoactive intestinal peptide; HSQC, heteronuclear single quantum coherence; DPC, dodecylphosphocholine; GPCR, G protein-coupled receptor; RA, rheumatoid arthritis; SAR, structure–activity relationship; TFE, trifluoroethanol

* Corresponding author at: Division of Structural Biology, Graduate School of Medicine, Kobe University, 7-5-1 Kusunoki-cho, Chuo-ku, Kobe, Hyogo 650-0017, Japan. Tel.: +81 78 382 5813; fax: +81 78 382 5816.
E-mail address: hiroakih@med.kobe-u.ac.jp (H. Hiroaki).

1570-9639/$ – see front matter © 2011 Elsevier B.V. All rights reserved.
doi:10.1016/j.bbapap.2011.03.009

of several cancers [17,18]. In cancers such as breast and prostate, an elevated expression of VPAC1 is observed [19]. Thus, accumulation of radio-labeled VIP analogs, such as ^{99m}Tc-labeled VIP and ^{64}Cu-labeled TP3939, enables visualization of cancers by positron emission tomography. VPAC receptors temporarily downregulate by endocytosis when VIP binds to them [20]. This mechanism has encouraged researchers to develop VIP analogs as imaging agents.

The 3D structure of VIP and its stability highlight the possible development of drug delivery systems with an improved therapeutic potency of VIP and its analogs. Several VIP formulations with increased biochemical and physicochemical stability have been studied extensively [21–23]. A typical variation for therapeutic VIPs is their incorporation into phospholipids or liposomes. Such variations generally double the activity of VIP. The primary benefit of the lipid/liposome formulation is to protect VIP from enzymatic degradation in vivo. In addition, a structural transition from a random coil to an α-helix on lipid and/or liposome binding is the rate-limiting step at the ligation of VIP to the receptors. A number of structural studies have shown that PACAP [24,25] as well as other class II GPCR ligands [26–29] adopt α-helical conformations when they bind to the receptor. A pre-existing α-helical conformation is also important in increasing the biological activities of the peptides [30], which is partly explained by a two-step model demonstrating the PACAP–PAC1R interaction [24]. Thus, the solution structure of VIP in the absence of its receptors and presence of phospholipids is another important issue.

In this study, we focused on the structural analysis of VIP in order to enable us to develop potent VIP analogs using a structure–activity relationship (SAR) study. Previously, the solution structure of VIP in 30% trifluoroethanol (TFE) solution was determined by the ^{1}H nuclear magnetic resonance (NMR) technique but not using isotopically labeled peptide [31], thereby showing limited structural convergence. In addition, the structural coordinates were not commonly available, thus limiting SAR studies by other groups. Here we determined the solution structures of VIP-G (28-residue VIP with extra C-terminal glycine, an equivalent peptide of the biosynthetic precursor of VIP before C-terminal amidation) in two different conditions, 50% MeOH, and aqueous buffer containing dodecylphosphocholine (DPC) micelles. Use of isotopically labeled VIP enabled analysis of the NMR spectra in the presence of a large number of DPC micelles in solution. Here we discuss the differences between the two structures in detail.

2. Materials and methods

2.1. Preparation of ^{15}N- and ^{13}C/^{15}N-labeled VIP-G

The bacterial expression system with VIP-G as the fusion protein of thioredoxin, followed by a 6-poly histidine tag, factor Xa cleavage site, and VIP-G [thioredoxin (TRX)_VIP-G], was as described previously [32]. For ^{15}N and ^{13}C/^{15}N labeling of the fusion protein TRX_VIP-G, M9 medium containing 0.5 g/L ^{15}N-NH_4Cl as the sole nitrogen source and 4 g/L of ^{12}C -glucose or 2 g/L of $^{13}C_6$-glucose, respectively, were used. *Escherichia coli* BL21(*DE3*) harboring pET-TRX_VIP-G was grown in 100 mL of M9 medium containing 50 μg/mL ampicillin for 16 h. The cells were transferred into 0.9 L cultures of the same medium in 5-L baffled flasks. Isopropyl-D-thiogalactopyranoside induction was performed as described earlier, except that the cells were incubated for 6 h at 30 °C prior to harvesting.

BL21(*DE3*) cells from 1 L of M9 medium were pelleted, resuspended in 30 mL of 50 mM Tris–HCl (pH 7.5), 0.15 M NaCl, and 10 mM mercaptoethanol, and disrupted by sonication. Cell debris were removed by centrifugation, and the extracts were then passed through a 4-mL column of DEAE-Sepharose. The extracts, cleared by either osmotic disruption or sonication, were loaded onto a 4-mL column of fast-flow chelating Sepharose, previously charged with 50 mM $NiSO_4$, and equilibrated in 20 mM imidazole and 50 mM Tris–HCl (pH 7.5). The column was then washed with 50 mM imidazole and 50 mM Tris–HCl (pH 7.5), followed by fusion protein elution with 0.2 M of imidazole and 50 mM Tris–HCl (pH 7.5). Fusion proteins eluted from the column (2 mL) were dialyzed against 1 L buffer containing 0.5 M NaCl and 50 mM Tris–HCl (pH 7.5) at 4 °C for 16 h.

2.2. NMR spectroscopy

NMR experiments were performed on a Bruker AvanceDRX (500 MHz) or an Bruker Avance III (600 MHz) NMR spectrometer, the latter being equipped with a cryogenic triple-resonance probe. To determine the structure in MeOH, ~400 μg of ^{13}C/^{15}N-VIP-G was dissolved in 0.25 mL of 50%–50% H_2O–d_3-MeOH containing 20 mM Tris–HCl (pH 7.4). For structural determination in a DPC micelle, ~500 μg of ^{15}N- or ^{13}C/^{15}N-VIP-G was dissolved in 0.25 mL of 90%–10% H_2O–D_2O containing 50 mM potassium phosphate buffer at pH 7.2, with and without 50 mM DPC micelle. Sodium 2,2-dimethyl-2-silapentane-5-sulfonate was used as a reference for the chemical shift. Heteronuclear single quantum coherence (HSQC) spectra [33] adapted with a gradient sensitivity enhancement [34] were acquired with eight transients and 256 increments at 288 or 298 K, and zero filling during spectral processing. All NMR spectra were recorded at 288 (in MeOH) or 298 K (in DPC micelle). All spectra were processed using NMRPipe [35] and analyzed using the program nmrDraw [35]. Interproton distances were obtained from 3D ^{13}C- and ^{15}N-edited HSQC NOESY spectra recorded with a 200-ms (in MeOH) and 150-ms (in DPC micelle) mixing time. Structures were calculated using a standard seven iteration cycle protocol of the program CYANA version 2.0.17 [36,37]. All NOE cross-peaks were selected manually using SPARKY [38]. Dihedral angle restraints were calculated using the TALOS program based on backbone atom chemical shifts [39]. The structural coordinates were deposited to PDB (PDB ID: 2RRH for the structure in MeOH), (PDB ID: 2RRI for the micelle-bound VIP), and the assignments were deposited to BMRB (accession numbers = 11419 and 11420, respectively).

3. Results and discussion

3.1. Structure of VIP-G in 50% MeOH

Organic solvents such as MeOH or TFE have been used in conformational studies of VIP and its derivatives by CD and/or NMR analysis to determine their SARs. These solvents, either neat or mixed with water, mimic hydrophobic environments, such as the cell membrane or N-terminal ectodomain (N-ted) of VIP receptors. Wild-type VIP is a 28-amino acid peptide having a C-terminal amide moiety. However, Fahrenkrug and co-workers clearly showed that the amide group of the C-terminus of VIP was not very effective for receptor binding or activation [40]. Therefore, glycine-extended VIP (VIP-G) (Fig. 1A) was used for the NMR analysis in this study. We employed ^{13}C/^{15}N isotopically labeled VIP-G produced by *E. coli*.

Assignments for the backbone HN, N, Cα, Cβ, and Co resonances of VIP-G in 50% MeOH were achieved by analysis of the triple-resonance HNCACB, CBCA(CO)NH, and HNCO spectra according to the standard method [41]. Hα, the side-chain proton, and carbon resonances were assigned from the HCC(CO)NH and CC(CO)NH spectra. Fig. 1B shows the assigned ^{1}H-^{15}N HSQC spectra of VIP-G in 50% MeOH. All backbone resonances, except for His^{1} and Ser^{2}, and 93% of the nonexchangeable protons of the side-chain signals were assigned. Backbone dihedral angle restraints were determined using the TALOS program [39]. TALOS showed an α-helix in VIP-G between Ala^{4} and Ser^{25} in 50% MeOH.

The final ensemble of 20 low-energy structures of VIP-G in 50% MeOH was generated from a total of 395 experimental constraints derived by NMR. Many medium-range NOEs showing helix, $d_{\alpha N}(i, i+3)$, $d_{\alpha\beta}(i, i+3)$, and $d_{\alpha N}(i, i+4)$ were observed among residues Val^{5}–Gly^{29} (Supplementary Fig. 1A). The RMSD values of the backbone atoms evaluated for Ala^{4}–Asn^{28} of the 20 structures were 0.35 Å for the

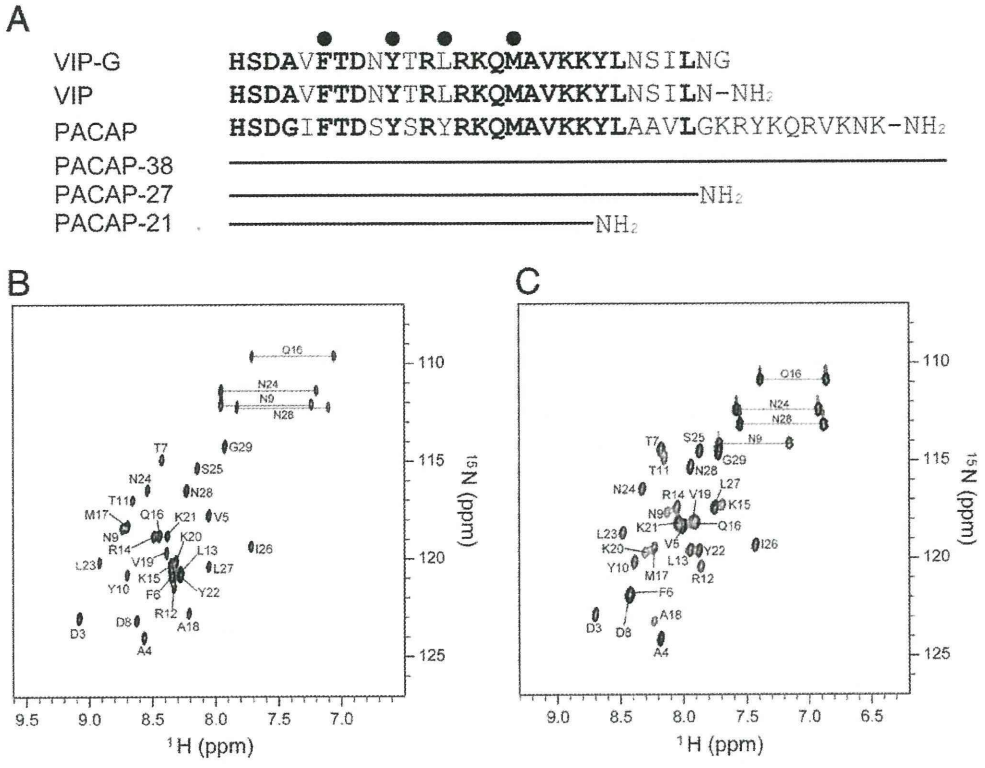

Fig. 1. Amino acid sequence and ^{1}H-^{15}N HSQC spectra. (A) Amino acid sequence of VIP and PACAP. Conserved residues are shown in bold. The filled circles indicate the residues forming a hydrophobic surface facing to DPC micelle. (B) and (C) ^{1}H-^{15}N HSQC spectra in 50% MeOH containing 20 mM Tris-HCl (pH 4.4) at 288 K (B) and in the presence of the 50 mM DPC micelle containing 50 mM potassium phosphate buffer (pH 7.2) at 298 K (C). Spectral cross-peaks are labeled by a 1-letter amino acid code and residue number.

backbone atoms and 0.95 Å for all the heavy atoms. The Ramachandran plot for all refined 20 structures for VIP-G shows that the backbone dihedral angles occupy the most favored or additionally allowed regions (Table 1). Superposition of the backbones of the 20 lowest target function structures in 50% MeOH is shown in Fig. 2. The structure of VIP-G in MeOH contains a central α-helix region comprising residues 4–29 and unstructured N-terminal regions (residues 1–3) (Fig. 2B).

Tan et al. previously reported the structure of VIP in 30% TFE [31]. The α-helical contents in 50% MeOH are similar to that in 30% TFE, which is also consistent with CD data. In contrast, the side-chain conformation is different in 50% MeOH and 30% TFE. In 30% TFE, several side-chain–side-chain interactions have been reported (Asn^{9}–Arg^{12}, Leu^{13}–Met^{17}, Val^{19}–Leu^{23}, and Lys^{20}–Asn^{24}). However, there were no side-chain interactions in this experiment, although the side-chain structure is well converged (RMSD values <1.0 Å).

Table 1
Structural statistics for the final 20 structures of VIP in DPC and 50% MeOH.

	MeOH	DPC
Distance restraints		
Total number of NOE restraints	395	376
Intraresidue	Unused	Unused
Sequential restraints ($\|i-j\|=1$)	246	246
Medium-range restraints ($1<\|i-j\|\leq 4$)	149	129
Long-range restraints ($\|i-j\|>5$)	0	1
Dihedral angle restraints		
$\varphi/\psi/\chi$	23/23/0	22/22/0
Hydrogen bond restraints	0	0
Final statistics		
Maximum target function	0.05	0.47
RMSD for experimental structure (Å)		
All backbone atoms (4–28 in MeOH, 6–26 in DPC)	0.35	0.55
All heavy atoms (4–28 in MeOH, 6–26 in DPC)	0.93	0.93
Ramachandran plot statistics (%)		
Most favored region	97.0	89.1
Additionally allowed region	3.0	10.9
Generously allowed region	0.0	0.0
Disallowed region	0.0	0.0

3.2. Structure of VIP-G bound to DPC micelle

We then determined the solution structure of VIP-G in the presence of the 50 mM DPC micelle (peptide/DPC ratio, 1:84). DPC is a well-known membrane-mimicking compound and is often used in solution NMR studies of peptide–membrane interactions. A DPC micelle is composed of ~60 DPC molecules in water. DPC has a neutral head group and mimics the nonisotropic environment of a lipid membrane. DPC forms stable micelles, resulting in reasonable correlation time and manageable line width for solution NMR studies. A remarkable difference in the DPC micelle compared with planar lipid bilayers is that the micelles possess a highly curved surface.

The ^{1}H-^{15}N HSQC spectra of VIP-G in the presence of DPC micelles are shown in Fig. 1C. We observed broader cross-peaks on the association of VIP-G to the DPC micelles (molecular mass of the DPC micelle is approximately 20 kDa). When more DPC was added to this sample (peptide/micelle ratio, 1:3), NMR signals were unchanged. Therefore, these NMR signals were from only the bound form within this experimental condition. We assigned all backbone resonances, except for His^{1} and Ser^{2}, and 93% of the nonexchangeable protons of the side-chain signals. An ensemble of 20 structures with low CYANA target functions was constructed from 376 experimental NMR constraints. The RMSD values after superimposing backbone atoms of Phe^{6}–Ile^{26} were 0.55 Å and 0.93 Å for backbone and heavy atoms, respectively. The secondary structure of the micelle-bound VIP-G consisted of an α-helix around Phe^{6}–Ile^{26} (Fig. 3). The N-terminal

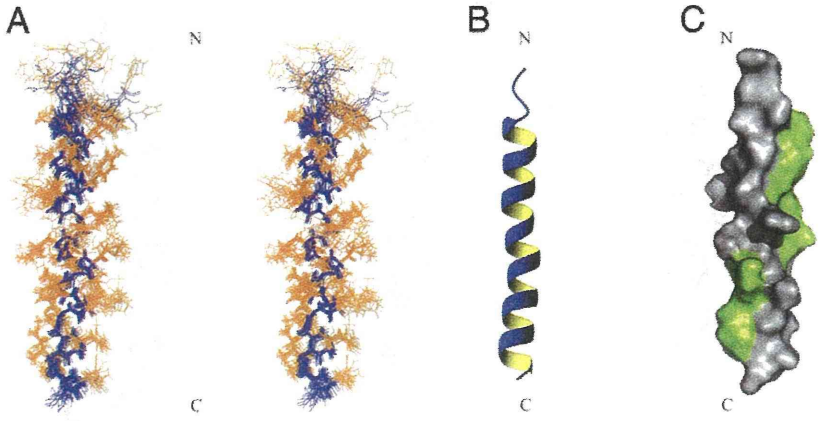

Fig. 2. Three-dimensional structures of VIP-G in 50% MeOH. (A) Ensemble of the 20 lowest energy structures of VIP-G in 50% MeOH. The backbone atoms of residues 4–28 were used for the superimposition. (B) and (C) Side views of the ribbon diagram (B) and surface model (C) of VIP-G of a representative conformer. The hydrophobic residues (V, I, L, Y, F, M) are colored green.

region (residues 1–5) was largely disordered, whereas the C-terminal region was more restricted and was close to an α-helical structure.

3.3. Comparison of 50% MeOH- and DPC micelle-bound forms of the VIP-G structure

To determine the interaction at the peptide–membrane interface, we first compared the chemical shift of VIP-G in DPC micelle to that in MeOH. Although the chemical shifts of several peaks were different in DPC and in MeOH, we could not determine the interaction at the VIP-G–micelle interface specifically from the chemical shift data. However, we determined the 3D structure of VIP-G in two different membrane-mimicking environments allowing us to compare two structures. Mapping of the hydrophobic residues on the molecular surface of VIP-G reveals that two hydrophobic patches are located at the opposite side of molecule (Figs. 2C and 3C). Compared with the structure of VIP-G in 50% MeOH, the α-helix of the micelle-bound form displayed a slight curvature (Fig. 4A and B). The diameter of this curvature was 21.84 ± 2.01 Å, which is similar to the reported size of a DPC micelle (Supplementary Fig. 2) [42]. The side chains of residues Phe^{6}, Tyr^{10}, Leu^{13}, and Met^{17} found at the concave face formed a hydrophobic patch in the micelle-bound state. VIP-G localized at the water–micelle boundary with these side chains toward the micelle interior. Thus, we inferred that this structural difference between the MeOH form and the micelle-bound form was caused by the peptide–micelle interaction on the curved micelle surfaces. Note that these two hydrophobic clusters were largely conserved within VIP and PACAP, which suggests the biological importance of the residues. The hydrophobic cluster consists of Ala^{18}, Val^{19}, Tyr^{22}, Leu^{23}, Ile^{26}, and Leu^{27} located at the peptide–N-ted interface on the structure of PACAP–PAC1R complex [25]. It is party consistent with an extensive SAR study on VIP, in which Ala-substituted mutants for each residue were examined [43]. Of course, direct proof of the peptide–lipid interaction of these residues requires further investigation by NMR experiments using spin-labeled DPC analogs.

3.4. Comparison of the structure of VIP-G and PACAP

The micelle- and receptor-bound structure of PACAP, which has high sequence homology with VIP, has been reported previously [24]. In this section, we compare our MeOH and micelle-bound forms of the VIP structure with other reported structures. Inooka et al. published a preliminary analysis of the micelle-bound structure of PACAP27, which adopts an α-helix (data not deposited on PDB). In addition, the micelle-bound structure of PACAP38 (PDB ID 2D2P), which comprises the flexible N-terminus (residues 1–4) followed by the

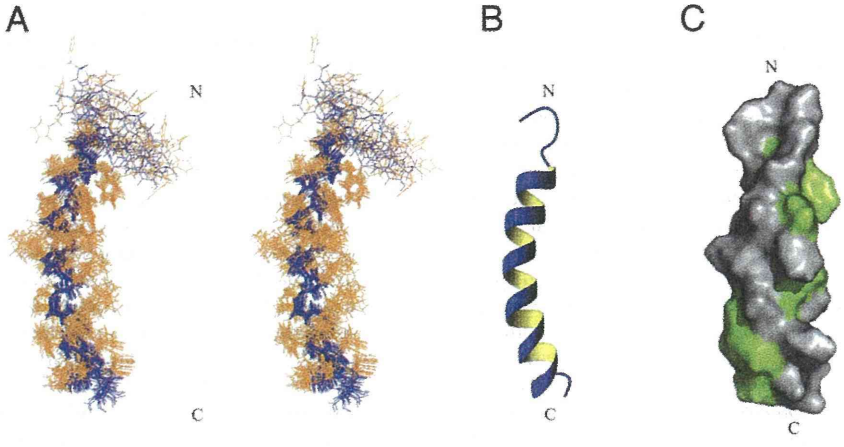

Fig. 3. Three-dimensional structures of VIP-G bound to a DPC micelle. (A) Ensemble of the 20 lowest energy structures of VIP-G in the DPC micelle. The backbone atoms of residues 6–26 were used for the superimposition. (B) and (C) Side views of the ribbon diagram (B) and surface model (C) of micelle-bound VIP-G of a representative conformer. The hydrophobic residues (V, I, L, Y, F, M) are colored green.

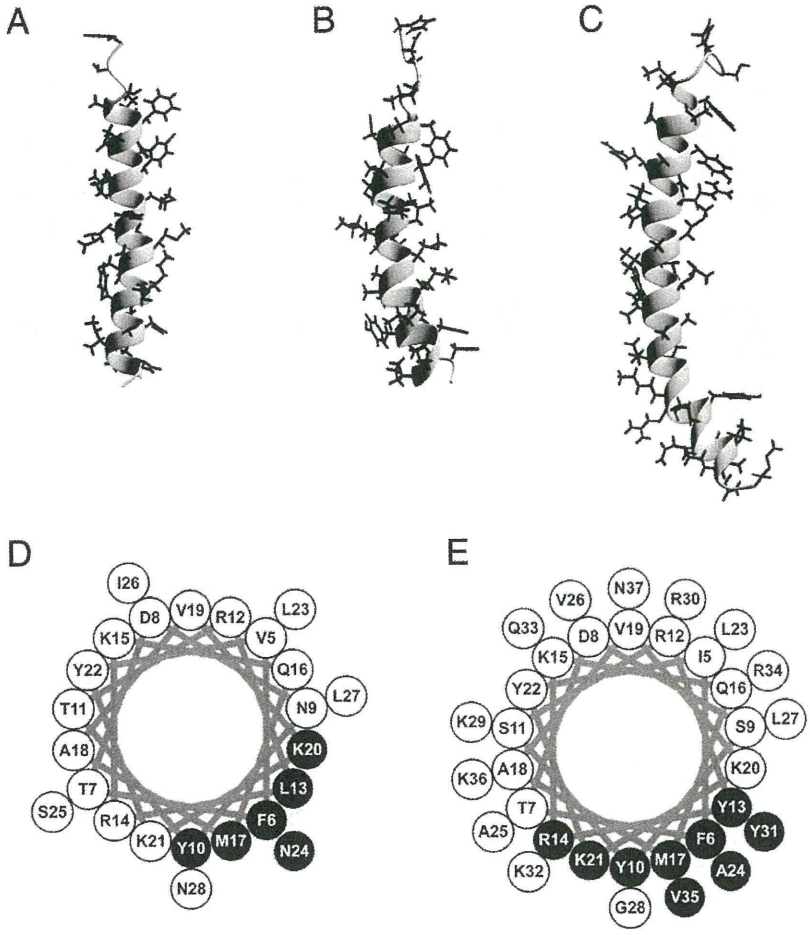

Fig. 4. Comparison of the structure of VIP-G and PACAP-38. (A–C) Side views of the ribbon diagram of VIP-G (in MeOH (A) and in the DPC micelle (B)) and PACAP-38 bound to the DPC micelle (C). (D and E) A helical wheel projections of the membrane-bound states of VIP (D) and PACAP (E). Amino acid residues located the peptide–membrane interface are shown in black.

stable α-helical region (5–38), is substantially similar to that of VIP-G (Fig. 4B and C). In particular, the C-terminal region of PACAP38 adopts a curved helix, which may reflect the curvature of the micelle. Moreover, the identical hydrophobic side chains (Phe^{6}, Tyr^{10}, Leu^{13}, and Met^{17}) form a micelle-binding interface inserted into the hydrophobic interior of the DPC micelle (Fig. 4D and E). This result indicates that VIP-G and PACAP have the same micelle-anchoring topology.

The conformations of VIP and PACAP in the lipid bilayer have also been studied, providing a better model for mimicking a cell membrane. A dimyristoylphosphatidylcholine/dimyristoylphosphatidylglycerol-based lipid bilayer was used as the peptide carrier to determine the structure of PACAP21 and PACAP27 using solid state NMR [44]. Interestingly, PACAP21 and PACAP27 adopted extended structures in the lipid bilayer-bound state. Gololobov et al. studied the conformation of VIP in liposomes using CD spectra and showed that VIP forms an α-helix in the presence of anionic phospholipid phosphatidylglycerol, whereas VIP remains unstructured in the presence of the neutral phospholipid phosphatidylcholine [30]. Although class II GPCR ligands usually adopt α-helices in the membrane-mimicking environment, VIP and PACAP vary their conformation depending on the environment, which might be unique. Considering the stable α-helical formation with an anionic lipid bilayer, some conserved cationic residues (Arg^{14}, Lys^{20}, and Lys^{21}) located near the peptide–micelle interface may play an important part in the conformational transition and α-helical stabilization.

3.5. Two-step ligand transportation mechanism of VIP in GPCR activation

As mentioned previously, the biological action of class II GPCR ligands is because of the ligation of peptides to the N-ted of the receptors. All the examples showed that these ligand peptides adopt an α-helical conformation on binding to the N-ted. A two-step ligand transportation model of GPCR activation was suggested [24,45]. Their model proposed that membrane interaction is an important event preceding receptor binding (Fig. 5). Peptide–membrane interaction induces an α-helical conformation closely homologous to the active one, leading to reduced losses in entropy upon receptor binding.

SAR was investigated by analyzing the biological activities of several variants of VIP. In particular, alanine-scanning studies revealed the key residues for VIP receptor binding or activation [43,46–48]. Modeling of the VIP structure in membrane-mimicking environments or with the receptor was also challenged [31,49]. Unfortunately, the interpretations of the existing pharmacological studies seemed to be controversial and did not succeed in perfectly explaining the mode of VIP action. Therefore, more structural information on VIP is required. In this study, we determined the micelle-bound VIP structure and found that four residues form a hydrophobic interface with the DPC micelle. Mutation on some of these residues showed substantial reduction in the activity of VIP, probably because they destabilized the α-helix. Thus, the residues in the peptide–membrane interface and those in the peptide–receptor interface must be separately considered in a SAR study.

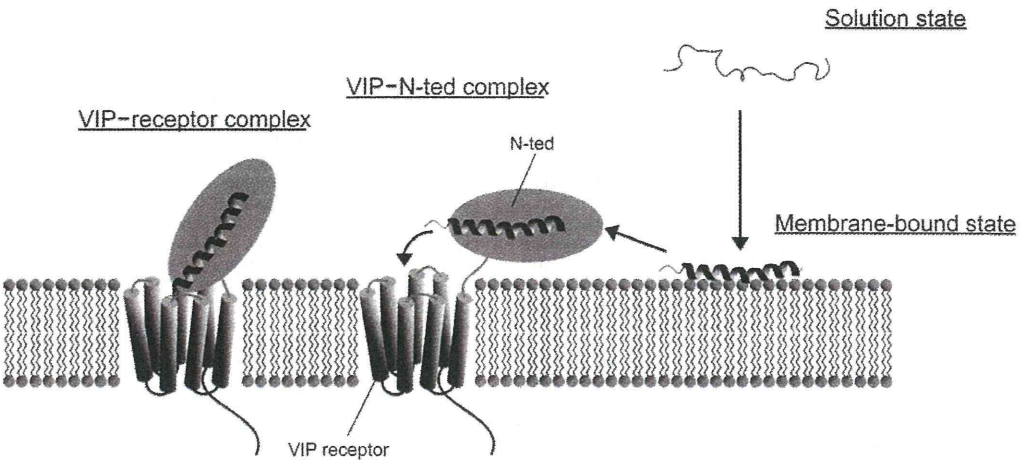

Fig. 5. Schematic diagram of the two-step ligand transportation model for VIP. The peptide nonspecifically binds to cell membranes and forms an α-helix at the C-terminal region. Then, VIP undergoes 2D diffusion to the receptor and binds to the N-ted of the VIP receptor. Finally, VIP is sandwiched between the N-ted and core of the receptor.

In conclusion, we have determined the solution structure of VIP in two distinct membrane-mimicking environments, both of which induced an α-helix in VIP. The data presented here will provide a rational basis for the development of VIP analogs, which will be useful in therapy for inflammatory diseases as well as cancer diagnoses.

Supplementary materials related to this article can be found online at doi:10.1016/j.bbapap.2011.03.009.

References

[1] B.H. Du, J. Eng, J.D. Hulmes, M. Chang, Y.C. Pan, R.S. Yalow, Guinea pig has a unique mammalian VIP, Biochem. Biophys. Res. Commun. 128 (1985) 1093–1098.
[2] S. Onoue, S. Misaka, S. Yamada, Structure–activity relationship of vasoactive intestinal peptide (VIP): potent agonists and potential clinical applications, Naunyn Schmiedebergs Arch. Pharmacol. 377 (2008) 579–590.
[3] M. Laburthe, A. Couvineau, V. Tan, Class II G protein-coupled receptors for VIP and PACAP: structure, models of activation and pharmacology, Peptides 28 (2007) 1631–1639.
[4] R.M. Campbell, C.G. Scanes, Evolution of the growth hormone-releasing factor (GRF) family of peptides, Growth Regul. 2 (1992) 175–191.
[5] G.V. Segre, S.R. Goldring, Receptors for secretin, calcitonin, parathyroid hormone (PTH)/PTH-related peptide, vasoactive intestinal peptide, glucagonlike peptide 1, growth hormone-releasing hormone, and glucagon belong to a newly discovered G-protein-linked receptor family, Trends Endocrinol. Metab. 4 (1993) 309–314.
[6] S.R. Rawlings, M. Hezareh, Pituitary adenylate cyclase-activating polypeptide (PACAP) and PACAP/vasoactive intestinal polypeptide receptors: actions on the anterior pituitary gland, Endocr. Rev. 17 (1996) 4–29.
[7] M. Laburthe, M. Rousset, C. Boissard, G. Chevalier, A. Zweibaum, G. Rosselin, Vasoactive intestinal peptide: a potent stimulator of adenosine 3':5'-cyclic monophosphate accumulation in gut carcinoma cell lines in culture, Proc. Natl Acad. Sci. U.S.A. 75 (1978) 2772–2775.
[8] R. Salomon, A. Couvineau, C. Rouyer-Fessard, T. Voisin, D. Lavallee, A. Blais, D. Darmoul, M. Laburthe, Characterization of a common VIP-PACAP receptor in human small intestinal epithelium, Am. J. Physiol. 264 (1993) 294–300.
[9] C.J. MacKenzie, E.M. Lutz, D.A. McCulloch, R. Mitchell, A.J. Harmar, Phospholipase C activation by VIP1 and VIP2 receptors expressed in COS 7 cells involves a pertussis toxin-sensitive mechanism, Ann. NY Acad. Sci. 805 (1996) 579–584.
[10] D.L. Bellinger, D. Lorton, S. Brouxhon, S. Felten, D.L. Felten, The significance of vasoactive intestinal polypeptide (VIP) in immunomodulation, Adv. Neuroimmunol. 6 (1996) 5–27.
[11] S.G. Smalley, P.A. Barrow, N. Foster, Immunomodulation of innate immune responses by vasoactive intestinal peptide (VIP): its therapeutic potential in inflammatory disease, Clin. Exp. Immunol. 157 (2009) 225–234.
[12] M. Kojima, T. Ito, T. Oono, T. Hisano, H. Igarashi, Y. Arita, K. Kawabe, D.H. Coy, R.T. Jensen, H. Nawata, VIP attenuation of the severity of experimental pancreatitis is due to VPAC1 receptor-mediated inhibition of cytokine production, Pancreas 30 (2005) 62–70.
[13] A. Arranz, C. Abad, Y. Juarranz, J. Leceta, C. Martinez, R.P. Gomariz, Vasoactive intestinal peptide as a healing mediator in Crohn's disease, Neuroimmunomodulation 15 (2008) 46–53.
[14] E. Gonzalez-Rey, M. Delgado, Therapeutic treatment of experimental colitis with regulatory dendritic cells generated with vasoactive intestinal peptide, Gastroenterology 131 (2006) 1799–1811.
[15] M. Delgado, C. Martinez, D. Pozo, J.R. Calvo, J. Leceta, D. Ganea, R.P. Gomariz, Vasoactive intestinal peptide (VIP) and pituitary adenylate cyclase-activation polypeptide (PACAP) protect mice from lethal endotoxemia through the inhibition of TNF-alpha and IL-6, J. Immunol. 162 (1999) 1200–1205.
[16] M. Delgado, C. Abad, C. Martinez, J. Leceta, R.P. Gomariz, Vasoactive intestinal peptide prevents experimental arthritis by downregulating both autoimmune and inflammatory components of the disease, Nat. Med. 7 (2001) 563–568.
[17] M.L. Thakur, C.S. Marcus, S. Saeed, V. Pallela, C. Minami, L. Diggles, H. Le Pham, R. Ahdoot, E.A. Kalinowski, 99mTc-labeled vasoactive intestinal peptide analog for rapid localization of tumors in humans, J. Nucl. Med. 41 (2000) 107–110.
[18] M.L. Thakur, M.R. Aruva, J. Gariepy, P. Acton, S. Rattan, S. Prasad, E. Wickstrom, A. Alavi, PET imaging of oncogene overexpression using 64Cu-vasoactive intestinal peptide (VIP) analog: comparison with 99mTc-VIP analog, J. Nucl. Med. 45 (2004) 1381–1389.
[19] J.C. Reubi, In vitro identification of vasoactive intestinal peptide receptors in human tumors: implications for tumor imaging, J. Nucl. Med. 36 (1995) 1846–1853.
[20] C. Boissard, J.C. Marie, G. Hejblum, C. Gespach, G. Rosselin, Vasoactive intestinal peptide receptor regulation and reversible desensitization in human colonic carcinoma cells in culture, Cancer Res. 46 (1986) 4406–4413.
[21] I. Rubinstein, Human VIP-alpha: an emerging biologic response modifier to treat primary pulmonary hypertension, Expert Rev. Cardiovasc. Ther. 3 (2005) 565–569.
[22] V. Sethi, H. Onyuksel, I. Rubinstein, Liposomal vasoactive intestinal peptide, Meth. Enzymol. 391 (2005) 377–395.
[23] F. Hajos, B. Stark, S. Hensler, R. Prassl, W. Mosgoeller, Inhalable liposomal formulation for vasoactive intestinal peptide, Int. J. Pharm. 357 (2008) 286–294.
[24] H. Inooka, T. Ohtaki, O. Kitahara, T. Ikegami, S. Endo, C. Kitada, K. Ogi, H. Onda, M. Fujino, M. Shirakawa, Conformation of a peptide ligand bound to its G-protein coupled receptor, Nat. Struct. Biol. 8 (2001) 161–165.
[25] C. Sun, D. Song, R.A. Davis-Taber, L.W. Barrett, V.E. Scott, P.L. Richardson, A. Pereda-Lopez, M.E. Uchic, L.R. Solomon, M.R. Lake, K.A. Walter, P.J. Hajduk, E.T. Olejniczak, Solution structure and mutational analysis of pituitary adenylate cyclase-activating polypeptide binding to the extracellular domain of PAC1-RS, Proc. Natl Acad. Sci. U.S.A. 104 (2007) 7875–7880.
[26] C.R. Grace, M.H. Perrin, J. Gulyas, M.R. Digruccio, J.P. Cantle, J.E. Rivier, W.W. Vale, R. Riek, Structure of the N-terminal domain of a type B1 G protein-coupled receptor in complex with a peptide ligand, Proc. Natl Acad. Sci. U.S.A. 104 (2007) 4858–4863.
[27] S. Runge, H. Thogersen, K. Madsen, J. Lau, R. Rudolph, Crystal structure of the ligand-bound glucagon-like peptide-1 receptor extracellular domain, J. Biol. Chem. 283 (2008) 11340–11347.
[28] C. Parthier, M. Kleinschmidt, P. Neumann, R. Rudolph, S. Manhart, D. Schlenzig, J. Fanghanel, J.U. Rahfeld, H.U. Demuth, M.T. Stubbs, Crystal structure of the incretin-bound extracellular domain of a G protein-coupled receptor, Proc. Natl Acad. Sci. U.S.A. 104 (2007) 13942–13947.
[29] A.A. Pioszak, H.E. Xu, Molecular recognition of parathyroid hormone by its G protein-coupled receptor, Proc. Natl Acad. Sci. U.S.A. 105 (2008) 5034–5039.
[30] G. Gololobov, Y. Noda, S. Sherman, I. Rubinstein, J. Baranowska-Kortylewicz, S. Paul, Stabilization of vasoactive intestinal peptide by lipids, J. Pharmacol. Exp. Ther. 285 (1998) 753–758.
[31] Y.V. Tan, A. Couvineau, S. Murail, E. Ceraudo, J.M. Neumann, J.J. Lacapere, M. Laburthe, Peptide agonist docking in the N-terminal ectodomain of a class II G protein-coupled receptor, the VPAC1 receptor. Photoaffinity, NMR, and molecular modeling, J. Biol. Chem. 281 (2006) 12792–12798.
[32] T. Tenno, N. Goda, Y. Tateishi, H. Tochio, M. Mishima, H. Hayashi, M. Shirakawa, H. Hiroaki, High-throughput construction method for expression vector of peptides for NMR study suited for isotopic labeling, Protein Eng. Des. Sel. 17 (2004) 305–314.
[33] D. Neri, T. Szyperski, G. Otting, H. Senn, K. Wuthrich, Stereospecific nuclear magnetic resonance assignments of the methyl groups of valine and leucine in the DNA-binding domain of the 434 repressor by biosynthetically directed fractional 13C labeling, Biochemistry 28 (1989) 7510–7516.

[34] L.E. Kay, P. Keifer, T. Saarinen, Pure absorption gradient enhanced heteronuclear single quantum correlation spectroscopy with improved sensitivity, J. Am. Chem. Soc. 114 (1992) 10663–10665.
[35] F. Delaglio, S. Grzesiek, G.W. Vuister, G. Zhu, J. Pfeifer, A. Bax, NMRPipe: a multidimensional spectral processing system based on UNIX pipes, J. Biomol. NMR 6 (1995) 277–293.
[36] T. Herrmann, P. Guntert, K. Wuthrich, Protein NMR structure determination with automated NOE assignment using the new software CANDID and the torsion angle dynamics algorithm DYANA, J. Mol. Biol. 319 (2002) 209–227.
[37] P. Guntert, Automated NMR protein structure calculation, Prog. Nucl. Magn. Reson. Spectrosc. 43 (2003) 105–125.
[38] T. D. Goddard, D. G. Kneller, Sparky 3. San Francisco: University of California.
[39] G. Cornilescu, F. Delaglio, A. Bax, Protein backbone angle restraints from searching a database for chemical shift and sequence homology, J. Biomol. NMR 13 (1999) 289–302.
[40] J. Fahrenkrug, B. Ottesen, C. Palle, Non-amidated forms of VIP (glycine-extended VIP and VIP-free acid) have full bioactivity on smooth muscle, Regul. Pept. 26 (1989) 235–239.
[41] J. Cavanagh, W.J. Fairbrother III, A.G. Palmer, M. Rance, N.J. Skelton, Protein NMR Spectroscopy: Principles and Practice, 2nd Ed, Academic Press, San Diego, 2007, pp. 535–673.
[42] F. Chevalier, J. Lopez-Prados, P. Groves, S. Perez, M. Martin-Lomas, P.M. Nieto, Structure and dynamics of the conserved protein GPI anchor core inserted into detergent micelles, Glycobiology 16 (2006) 969–980.
[43] P. Nicole, L. Lins, C. Rouyer-Fessard, C. Drouot, P. Fulcrand, A. Thomas, A. Couvineau, J. Martinez, R. Brasseur, M. Laburthe, Identification of key residues for interaction of vasoactive intestinal peptide with human VPAC1 and VPAC2 receptors and development of a highly selective VPAC1 receptor agonist. Alanine scanning and molecular modeling of the peptide, J. Biol. Chem. 275 (2000) 24003–24012.
[44] N. Komi, K. Okawa, Y. Tateishi, M. Shirakawa, T. Fujiwara, H. Akutsu, Structural analysis of pituitary adenylate cyclase-activating polypeptides bound to phospholipid membranes by magic angle spinning solid-state NMR, Biochim. Biophys. Acta 1768 (2007) 3001–3011.
[45] S.R.J. Hoare, Mechanisms of peptide and nonpeptide ligand binding to Class B G-protein-coupled receptors, Drug Discov. Today 10 (2005) 417–427.
[46] M. O'Donnell, R.J. Garippa, N.C. O'Neill, D.R. Bolin, J.M. Cottrell, Structure–activity studies of vasoactive intestinal polypeptide, J. Biol. Chem. 266 (1991) 6389–6392.
[47] H. Igarashi, T. Ito, W. Hou, S.A. Mantey, T.K. Pradhan, C.D. Ulrich, S.J. Hocart, D.H. Coy, R.T. Jensen, Elucidation of vasoactive intestinal peptide pharmacophore for VPAC(1) receptors in human, rat, and guinea pig, J. Pharmacol. Exp. Ther. 301 (2002) 37–50.
[48] H. Igarashi, T. Ito, S.A. Mantey, T.K. Pradhan, W. Hou, D.H. Coy, R.T. Jensen, Development of simplified vasoactive intestinal peptide analogs with receptor selectivity and stability for human vasoactive intestinal peptide/pituitary adenylate cyclase-activating polypeptide receptors, J. Pharmacol. Exp. Ther. 315 (2005) 370–381.
[49] E. Ceraudo, S. Murail, Y.V. Tan, J.J. Lacapere, J.M. Neumann, A. Couvineau, M. Laburthe, The vasoactive intestinal peptide (VIP) alpha-helix up to C terminus interacts with the N-terminal ectodomain of the human VIP/Pituitary adenylate cyclase-activating peptide 1 receptor: photoaffinity, molecular modeling, and dynamics, Mol. Endocrinol. 22 (2008) 147–155.

^{1}H, ^{13}C, and ^{15}N resonance assignment of the first PDZ domain of mouse ZO-1

Yoshitaka Umetsu, Natsuko Goda, Ryo Taniguchi, Kaori Satomura, Takahisa Ikegami, Mikio Furuse & Hidekazu Hiroaki

Biomolecular NMR Assignments

ISSN 1874-2718
Volume 5
Number 2

Biomol NMR Assign (2011)
5:207-210
DOI 10.1007/s12104-011-9301-x

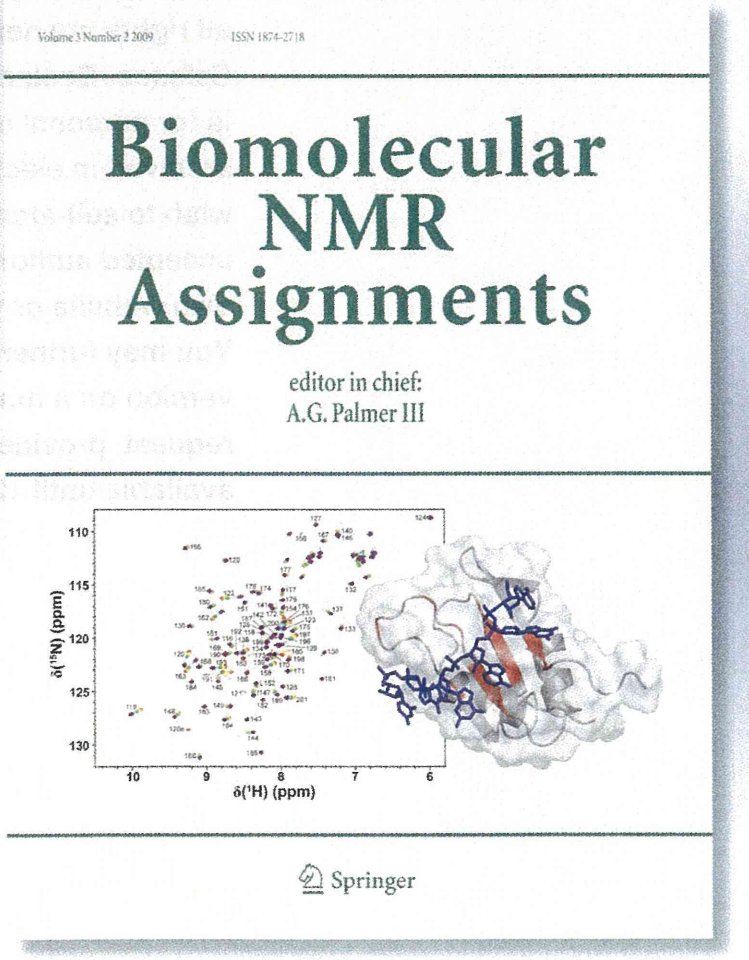

Springer

Biomol NMR Assign (2011) 5:207–210
DOI 10.1007/s12104-011-9301-x

ARTICLE

^{1}H, ^{13}C, and ^{15}N resonance assignment of the first PDZ domain of mouse ZO-1

Yoshitaka Umetsu · Natsuko Goda · Ryo Taniguchi · Kaori Satomura · Takahisa Ikegami · Mikio Furuse · Hidekazu Hiroaki

Received: 7 January 2011 / Accepted: 12 March 2011 / Published online: 24 March 2011

Abstract Zonula occludens-1 (ZO-1) is a scaffolding molecule critical to the formation of intercellular adhesion structures, such as tight junctions (TJs) and adherens junctions (AJs). ZO-1 contains three PDZ domains followed by a GUK domain and a ZU5 domain. The first PDZ of ZO-1 (ZO-1(PDZ1)) serves as a protein–protein interaction module and interacts with the C-termini of almost all claudins to initiate the formation of a belt-like structure on the lateral membranes, thereby promoting TJ formation. It has been recently reported that approximately 15% of all PDZ domains bind phosphoinositides, and ZO-1(PDZ1) is the one of these. Here we report the ^{15}N, ^{13}C, and ^{1}H chemical shift assignments of the first PDZ domain of mouse ZO-1. The resonance assignments obtained in this work may contribute in clarifying the interplay between the two binary interactions, ZO-1(PDZ1)–claudins and ZO-1(PDZ1)–phospholipids, and suggesting a novel regulation mechanism underlying the formation and maintenance of cell–cell adhesion machinery downstream of the phospholipid signaling pathways.

Keywords Cell–cell adhesion · Tight junction · ZO-1; PDZ domain · Phosphoinositide

Y. Umetsu · N. Goda · R. Taniguchi · K. Satomura · H. Hiroaki
Division of Structural Biology Graduate School of Medicine, Kobe University, Kobe, Hyogo, Japan

K. Satomura · M. Furuse · H. Hiroaki
Targeted Protein Research Program (JST-TPRP), Kobe University, Kobe, Hyogo, Japan

T. Ikegami
Institute for Protein Research, Osaka University, Suita, Osaka, Japan

M. Furuse · H. Hiroaki (✉)
Global-COE (Center of Excellence) Program for Integrative Membrane Biology, Kobe University, Kobe, Hyogo, Japan
e-mail: hiroakih@med.kobe-u.ac.jp

M. Furuse
Division of Cell Biology, Graduate School of Medicine, Kobe University, Kobe, Hyogo, Japan

Biological context

The tight junction (TJ), or zonula occludens, is the most apical intercellular junctional complex found in epithelial and endothelial cells. It is believed that TJs maintain the major epithelial and endothelial barrier functions, thus maintaining the unique composition of chemical and biological substances at the apical and basolateral spaces of the cell layer (Furuse et al. 1993; Ikenouchi et al. 2007). TJs are responsible for the formation of barriers regulating the passage of solutes and cells through the paracellular space. In addition to their semipermeable barrier and/or gate function, TJs are also involved in some signal transduction pathways, i.e., they regulate their own assembly and barrier function, as well as transmit signals from the paracellular space to the cell interior by coordinating a variety of signaling and trafficking molecules that regulate cell differentiation, proliferation, and polarity (Tsukita et al., 2001; Ikenouchi et al. 2005; Martin-Padura et al. 1998).

The extracellular part of TJs is composed of four families of integral membrane proteins, claudins (Furuse et al. 1998; Morita et al. 2003), occludin (Furuse et al. 1993), junctional adhesion molecules (JAMs) (Martin-Padura et al. 1998), and tricellulin (Ikenouchi et al. 2005). Most of these membrane proteins are linked to each other by PDZ (PSD95/Discs large/ZO-1) domain-containing scaffold proteins. The PDZ

domain is compact and globular. It is the most abundant peptide-binding module in the human genome, in which there may be as many as 440 PDZ domains in 259 different proteins (Letunic et al. 2004). In TJs, membrane-associated guanylate kinase (MAGUK) proteins, ZO-1, and ZO-2 are localized exclusively in polarized epithelia (Gonzalez-Mariscal et al. 2000; Gonzalez-Mariscal et al. 2003).

Here we describe the NMR assignments of the first PDZ domain of ZO-1, ZO-1(PDZ1). As well as most other PDZ domain-containing proteins, ZO-1 and ZO-2 are multiple tandem PDZ domains that harbor other protein-binding modules, such as SH3 and ZU5 domains, thereby functioning as a scaffold. One of the pivotal interactions in junctional complexes is that between the first PDZ domains from ZO-1 or ZO-2 and the cytosolic C-terminal PDZ-binding motif of claudins (Itoh et al. 1999). More recently, approximately 15% of PDZ domains were shown to interact with phospholipids directly (Wu et al. 2007; Zimmermann 2006), and ZO-1(PDZ1) and ZO-1(PDZ2) are examples in the case (Meerschaert et al. 2009). Thus, the resonance assignments of ZO-1(PDZ1) contribute to the study of the interactions between ZO-1(PDZ1) and claudins or other ligands, such as phosphoinositides.

Methods and experiments

Sample preparation

The expression vector for the recombinant GST-tagged form of mouse ZO-1(PDZ1) (residues 18–110) was constructed using PRESAT-vector methodology (Tenno et al. 2004). Isotopically labeled protein for NMR spectroscopy was generated in *Escherichia coli* BL21(*DE3*) from 1 L M9 minimal medium culture grown at 20°C in the presence of [^{15}N]-NH_4Cl and [^{13}C]-glucose as the sole nitrogen and carbon sources, respectively. The harvested cells were resuspended in lysis buffer (50 mM Tris–HCl, pH 7.5, 150 mM NaCl) and disrupted by sonication. The supernatant was applied to a DEAE-Sepharose (GE Healthcare) column and then affinity purified by Glutathione Sepharose 4 Fast Flow (GE Healthcare) chromatography. The GST tag was removed by PreScission protease on beads. Next, the ZO-1(PDZ1) was purified by gel filtration using a HiLoad 26/60 Superdex 75 pg (GE Healthcare). Using this purification protocol, ^{15}N-labeled or ^{13}C, ^{15}N-doubly-labeled ZO-1(PDZ1) was prepared. The purified protein was concentrated to 0.73 mM and dialyzed with 22 mM MES (pH5.9). The protein solution (313.5 μL) and 16.5 μL 99% D_2O were mixed, resulting in 0.7 mM ZO-1(PDZ1) in 20 mM MES (pH 5.9) in 95% H_2O–5% D_2O. ^{14}N-amino-acid-selective-inversely-labeled ^{15}N-labeled-ZO-1(PDZ1) was also prepared. (Arg^-)- and (Lys^-)-^{15}N-labeled-ZO-1(PDZ1) were prepared from 0.5 L ^{15}N-enriched M9 media supplemented with ^{14}N-Lys or ^{14}N-Arg, respectively. (The details of the protocol are in preparation.)

NMR spectroscopy

NMR experiments were performed on a Bruker AvanceDRX (600 MHz) or an Avance III (600 MHz) NMR spectrometer (Bruker), the latter was equipped with a cryogenic triple-resonance probe. For the assignment of backbone ^{1}H, ^{13}C, and ^{15}N resonances, HNCA, HN(CO)CA, HNCACB, CBCA(CO)NH, HNCO, HN(CA)CO, and 3D ^{15}N-edited-NOESY-HSQC spectra were recorded. For side chain resonance assignment, 2D constant-time ^{1}H-^{13}C HSQC, 3D ^{13}C-edited-NOESY-HSQC, HCCH-TOCSY, CC(CO)NNH, and HCC(CO)NNH spectra were recorded. All NMR spectra were recorded at 298 K. All spectra were processed using NMRPipe (Delaglio et al. 1995) and analyzed using the program SPARKY (Goddard and Kneller 2004).

Assignments and data deposition

The sequential assignment of backbone signals was initiated by the automatic program MARS (Jung and Zweckstetter 2004), resulting in approximately 60% completion. However, subsequent iterative MARS runs could not increase further assignment gains beyond 65%. We then carefully traced the sequential connectivities based on triple-resonance data sets. Further help with assignment was provided by the ^{15}N-edited NOESY spectra. These backbone assignments were confirmed by a visual inspection of ^{15}N-HSQC spectra of (Lys^- -/(Arg^-)- inversely labeled ZO-1(PDZ1).

Following a sequential assignment procedure, 94.7% of the $^1H^N$, ^{15}N resonances of the backbone amide groups (90 out of the 95 non-Pro residues) were assigned (Fig. 1). In addition, 93.0% of H^α (93 out of 100 residues), 94.0% of $^{13}C^\alpha$ (94 out of 100 residues), and 94.3% of $^{13}C^\beta$ (82 out of 87 residues) resonances were assigned. The secondary structure of ZO-1(PDZ-1) was predicted by comparing the chemical shifts with random coil values using TALOS program. This result and our preliminary structural analysis of ZO-1(PDZ-1) indicate six β-strands (Glu10-Leu16, Ile26-Ser29, Val45-Val49, Arg64-Val68, Val71-Ser72, and Ala92-Arg98) and an α-helix (Glu77-Lys87), in good agreement with the structural elements of crystal structure of ZO-1(PDZ-1) (PDB: 2H3 M) (Appleton et al. 2006). The sequential correlations of the backbone resonances of His36, Phe37, Gln38, and Ser39 were missing. On the ^{1}H-^{15}N HSQC spectra, there was only one unassigned main-chain amide proton resonance, which may correspond to one of these residues. The residues are involved in the long loop

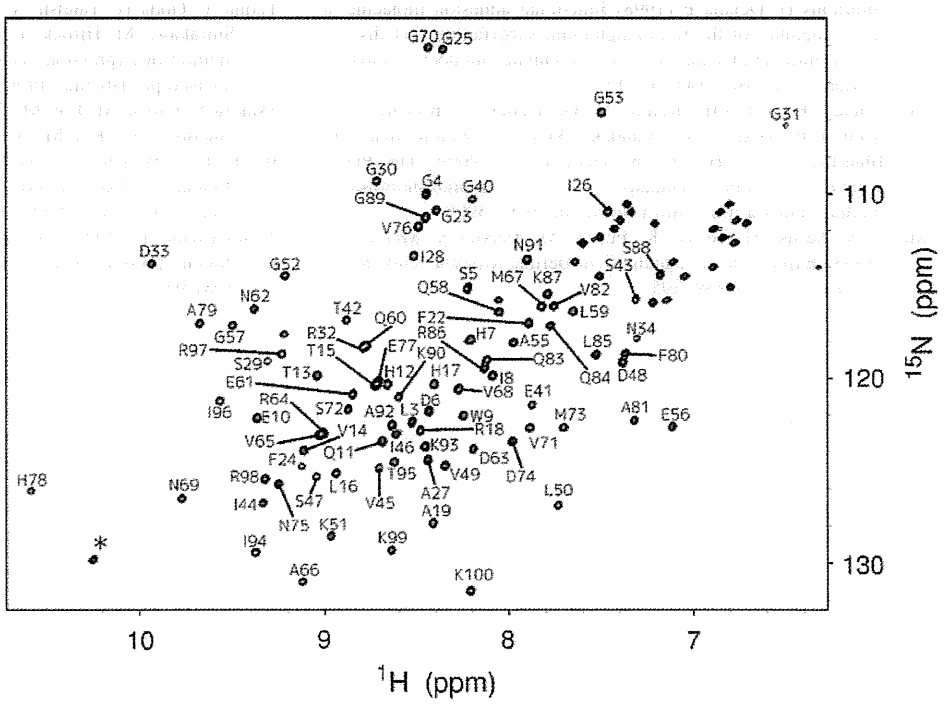

Fig. 1 A portion of the ^{15}N-^{1}H-HSQC spectrum of the first PDZ domain of mouse ZO-1 protein illustrating a number of the assigned backbone ^{15}N resonances. Asterisk indicates the Trp9 side chain

between $\beta 2$ and $\beta 3$. In the crystal structure of ZO-1(PDZ1), the loop adopted a compact L-like structure and was closed toward the $\beta 2$ surface. However, part of the loop had some contact with the neighboring molecule in the crystal lattice, suggesting that this folded structure may not be natural in solution. In our preliminary analysis of the solution structure of ZO-1(PDZ1), this folded loop structure was not observed (manuscript in preparation). It is likely that the loop, including the four "missing residues," adopts a loose, extended conformation in certain structural equilibrium.

Because of the sample preparation from the GST-fusion protein construct, the NMR sample must contain the extra seven residues (GPLGSDH) preceding the N-terminus in mouse ZO-1 (residues 18–110) in the sample. Thus, in the chemical shift data and Fig. 1, the residues 1–7 correspond to GPLGSDH from the expression vector, whereas the residues 8–100 are equivalent to the residues 18–110 of the full length mouse ZO-1. The assigned chemical shifts of ZO-1(PDZ1) have been deposited in the BioMagResBank under accession number 11424.

Acknowledgments This work was supported by a Grant-in-Aid from Bioinformatics Research and Development (BIRD) and Target Protein Research Program (TPRP) of the Japan Scientific and Technology Cooperation (JST).

References

Appleton BA, Zhang Y, Wu P, Yin JP, Hunziker W, Skelton NJ, Sidhu SS, Wiesmann C (2006) Comparative structural analysis of the Erbin PDZ domain and the first PDZ domain of ZO-1. Insights into determinants of PDZ domain specificity. J Biol Chem 281:22312–22320

Delaglio F, Grzesiek S, Vuister GW, Zhu G, Pfeifer J, Bax A (1995) NMRPipe: a multidimensional spectral processing system based on UNIX pipes. J Biomol NMR 6:277–293

Furuse M, Hirase T, Itoh M, Nagafuchi A, Yonemura S, Tsukita S, Tsukita S (1993) Occludin: a novel integral membrane protein localizing at tight junctions. J Cell Biol 123:1777–1788

Furuse M, Fujita K, Hiiragi T, Fujimoto K, Tsukita S (1998) Claudin-1 and -2: novel integral membrane proteins localizing at tight junctions with no sequence similarity to occludin. J Cell Biol 141:1539–1550

Goddard TD, Kneller DG (2004) Sparky 3. University of California, San Francisco

Gonzalez-Mariscal L, Betanzos A, Avila-Flores A (2000) MAGUK proteins: structure and role in the tight junction. Semin Cell Dev Biol 11:315–324

Gonzalez-Mariscal L, Betanzos A, Nava P, Jaramillo BE (2003) Tight junction proteins. Prog Biophys Mol Biol 81:1–44

Ikenouchi J, Furuse M, Furuse K, Sasaki H, Tsukita S, Tsukita S (2005) Tricellulin constitutes a novel barrier at tricellular contacts of epithelial cells. J Cell Biol 171:939–945

Ikenouchi J, Umeda K, Tsukita S, Furuse M, Tsukita S (2007) Requirement of ZO-1 for the formation of belt-like adherens junctions during epithelial cell polarization. J Cell Biol 176:779–786

Itoh M, Furuse M, Morita K, Kubota K, Saitou M, Tsukita S (1999) Direct binding of three tight junction-associated MAGUKs, ZO-1, ZO-2, and ZO-3, with the COOH termini of claudins. J Cell Biol 147:1351–1363

Jung YS, Zweckstetter M (2004) Mars–robust automatic backbone assignment of proteins. J Biomol NMR 30:11–23

Letunic I, Copley RR, Schmidt S, Ciccarelli FD, Doerks T, Schultz J, Ponting CP, Bork P (2004) SMART 4.0: towards genomic data integration. Nucleic Acids Res 32(Database issue):142–144

Martin-Padura I, Lostaglio S, Schneemann M, Williams L, Romano M, Fruscella P, Panzeri C, Stoppacciaro A, Ruco L, Villa A,

Simmons D, Dejana E (1998) Junctional adhesion molecule, a novel member of the immunoglobulin superfamily that distributes at intercellular junctions and modulates monocyte transmigration. J Cell Biol 142:117–127

Meerschaert K, Tun MP, Remue E, De Ganck A, Boucherie C, Vanloo B, Degeest G, Vandekerckhove J, Zimmermann P, Bhardwaj N, Lu H, Cho W, Gettemans J (2009) The PDZ2 domain of zonula occludens-1 and -2 is a phosphoinositide binding domain. Cell Mol Life Sci 66:3951–3966

Morita K, Sasaki H, Furuse K, Furuse M, Tsukita S, Miyachi Y (2003) Expression of claudin-5 in dermal vascular endothelia. Exp Dermatol 12:289–295

Tenno T, Goda N, Tateishi Y, Tochio H, Mishima M, Hayashi H, Shirakawa M, Hiroaki H (2004) High-throughput construction method of expression vector of peptides for NMR study suited for isotopic labeling. Protein Eng. Des. Sel. 17:305–314

Tsukita S, Furuse M, Itoh M (2001) Multifunctional strands in tight junctions. Nat Rev Mol Cell Biol 2:285–293

Wu H, Feng W, Chen J, Chan LN, Huang S, Zhang M (2007) PDZ domains of Par-3 as potential phosphoinositide signaling integrators. Mol Cell 28:886–898

Zimmermann P (2006) The prevalence and significance of PDZ domain-phosphoinositide interactions. Biochim Biophys Acta 1761:947–956

Published May 30, 2011

SH3YL1 regulates dorsal ruffle formation by a novel phosphoinositide-binding domain

Junya Hasegawa,[1] Emi Tokuda,[2] Takeshi Tenno,[3] Kazuya Tsujita,[2] Haruko Sawai,[1] Hidekazu Hiroaki,[3] Tadaomi Takenawa,[2] and Toshiki Itoh[1]

[1]Division of Membrane Biology, [2]Division of Lipid Biochemistry, and [3]Division of Structural Biology, Department of Biochemistry and Molecular Biology, Kobe University Graduate School of Medicine, Kobe, Hyogo 650-0017, Japan

Reversible interactions between cytosolic proteins and membrane lipids such as phosphoinositides play important roles in membrane morphogenesis driven by actin polymerization. In this paper, we identify a novel lipid-binding module, which we call the SYLF domain (after the SH3YL1, Ysc84p/Lsb4p, Lsb3p, and plant FYVE proteins that contain it), that is highly conserved from bacteria to mammals. SH3YL1 (SH3 domain containing Ysc84-like 1) strongly bound to phosphatidylinositol 3,4,5-triphosphate ($PI(3,4,5)P_3$) and several D5-phosphorylated phosphoinositides through its SYLF domain and was localized to circular dorsal ruffles induced by platelet-derived growth factor stimulation. Interestingly, SHIP2 (the $PI(3,4,5)P_3$ 5-phosphatase, src-homology 2–containing inositol-5-phosphatase 2) was identified as a binding partner of SH3YL1, and knockdown of these proteins significantly suppressed dorsal ruffle formation. Phosphatidylinositol 3,4-bisphosphate ($PI(3,4)P_2$), which is mainly synthesized from $PI(3,4,5)P_3$ by the action of SHIP2, was enriched in dorsal ruffles, and $PI(3,4)P_2$ synthesis strongly correlated with formation of the circular membrane structure. These results provide new insight into the molecular mechanism of dorsal ruffle formation and its regulation by phosphoinositide metabolism.

Introduction

Membrane ruffles are short-lived, highly dynamic, and F-actin–enriched structures induced by various extracellular stimuli. It is now well established that treatment with growth factors, including EGF and PDGF, results in the formation of two different types of plasma membrane structures: peripheral ruffles and dorsal ruffles (Buccione et al., 2004). Of these two structures, dorsal ruffles are easily distinguishable from peripheral ruffles by their unique ring-shaped morphology and are believed to play important roles in the establishment of polarity in motile cells, macropinocytosis, and the internalization of cell surface receptors (Dowrick et al., 1993; Warn et al., 1993; Swanson and Watts, 1995; Krueger et al., 2003; Orth and McNiven, 2006). For the formation of dorsal ruffles, engagement of the growth factors to their receptor tyrosine kinases activates early effector kinases such as phosphatidylinositol 3-kinase (PI3K) and Src. This leads to the activation of downstream signaling proteins, including small GTPases such as Rac, Ras, and Rab5 and serine/threonine kinases such as protein kinase A and Pak1 (Dharmawardhane et al., 2000; Lanzetti et al., 2004; Palamidessi et al., 2008). Consequently, these signaling pathways are thought to regulate the activity of cytoskeletal components such as neuronal Wiskott-Aldrich syndrome protein (N-WASP), Arp2/3, cortactin, sorting nexin 9, and dynamin for the robust actin polymerization at dorsal ruffles (Krueger et al., 2003; Buccione et al., 2004; Legg et al., 2007; Yarar et al., 2007). Despite these findings, the role of membrane lipids such as phosphoinositides and their metabolizing enzymes, including phosphoinositide kinases and phosphatases, is yet to be determined.

Reversible interactions between soluble cytosolic proteins and phospholipids in the plasma membrane are essential for a wide variety of cellular functions, including vesicular trafficking, cell proliferation, and motility (Itoh and Takenawa, 2002; Lemmon, 2008). Moreover, studies in recent years have revealed that the curvature of membranes can be determined by a certain group of lipid-binding modules such as Bin–Amphiphysin–Rvs (BAR), Fer-CIP4 homology and BAR (F-BAR), and Epsin N-terminal

Correspondence to Toshiki Itoh: titoh@med.kobe-u.ac.jp

Abbreviations used in this paper: BAR, Bin–Amphiphysin–Rvs; CBB, Coomassie brilliant blue; ENTH, Epsin N-terminal homology; N-WASP, neuronal Wiskott-Aldrich syndrome protein; PC, phosphatidylcholine; PE, phosphatidylethanolamine; PH, pleckstrin homology; $PI(3,4)P_2$, phosphatidylinositol 3,4-bisphosphate; $PI(3,4,5)P_3$, phosphatidylinositol 3,4,5-triphosphate; PI3K, phosphatidylinositol 3-kinase; SVM, support vector machine.

Supplemental Material can be found at:
http://jcb.rupress.org/content/suppl/2011/05/26/jcb.201012161.DC1.html

The Rockefeller University Press $30.00
J. Cell Biol. Vol. 193 No. 5 901–916
www.jcb.org/cgi/doi/10.1083/jcb.201012161

Published May 30, 2011

homology (ENTH) domains (McMahon and Gallop, 2005; Itoh and De Camilli, 2006; Heath and Insall, 2008). These domains not only bind to acidic phospholipids but can also transform $PI(4,5)P_2$-containing liposomes into elongated membrane tubules in vitro (Takei et al., 1999; Farsad et al., 2001; Ford et al., 2002; Itoh et al., 2005; Tsujita et al., 2006). In addition, overexpression of these domains can also induce robust tubular invaginations of the plasma membrane in the cell (Lee et al., 2002; Kamioka et al., 2004). The BAR domain super family proteins, including those with the BAR and F-BAR domains, typically contain a single or tandem SH3 domains at their C termini to form a molecular complex with N-WASP and dynamin, two key components in actin polymerization and membrane fission during clathrin-mediated endocytosis (Ringstad et al., 1997; Itoh et al., 2005; Tsujita et al., 2006).

Here, we describe a novel phosphoinositide-binding domain in a group of proteins with a C-terminal SH3 domain named the SYLF (SH3YL1, Ysc84p/Lsb4p, Lsb3p, and plant FYVE protein) domain. The SYLF domain of an SH3 domain containing Ysc84-like 1 (SH3YL1), a mammalian protein, strongly binds to D5-phosphoinositides including phosphatidylinositol 3,4,5-triphosphate ($PI(3,4,5)P_3$). We further identify the $PI(3,4,5)P_3$ 5-phosphatase src-homology 2–containing inositol-5-phosphatase 2 (SHIP2) as a binding partner for SH3YL1, and both proteins are required for the formation of circular dorsal ruffles induced by PDGF stimulation. Phosphatidylinositol 3,4-bisphosphate ($PI(3,4)P_2$), which is synthesized from $PI(3,4,5)P_3$ by the action of SHIP2, is enriched at matured dorsal ruffles, indicating that this phosphoinositide transition plays an important role in the formation of the ring-shaped membrane structure. Our findings suggest a mechanism by which SH3YL1 couples SHIP2 as well as subsequent $PI(3,4)P_2$ synthesis for membrane remodeling during dorsal ruffle formation.

Results

The N-terminal region of SH3YL1 is an evolutionarily conserved and structurally independent domain with high affinity for phosphoinositides

While searching the Pfam database for proteins with an SH3 domain in their C termini, we identified an unexplored domain species, domain of unknown function (DUF) 500. By sequence alignment, we found that the DUF500 domain is part of a longer amino acid sequence that is conserved from yeast to mammals (Fig. S1 A). Notably, this homologous region exists not only in eukaryotes, such as fungi, plants, and vertebrates, but also in Gram-negative bacteria (see Discussion).

To determine whether this entire region forms an independent structure that extends from the DUF500 domain to the N terminus, we predicted the domain boundary by using the support vector machine (SVM) long method (Ebina et al., 2009). In the primary sequence of human SH3YL1 (Aoki et al., 2000), a putative linker region separating two structural domains was predicted to be Gln230–Glu265 with a peak probability at Pro242 (Fig. 1 A), suggesting that ~230 N-terminal residues form a structurally independent unit. A similar result was obtained using the DomCut server (Suyama and Ohara, 2003), which predicted Pro246 as the most probable linker position (unpublished data). These predictions were supported by the results of proteolytic digestion experiments, wherein purified FLAG-SH3YL1 (full length) protein was incubated with limiting amounts of trypsin. The N-terminal region of SH3YL1, which was recognized by anti-FLAG, was cleaved to an ~25-kD fragment, slightly larger than FLAG-SH3YL1 SYLF (1–216) (Fig. 1 B). A faint band was also observed around ~16 kD (Fig. 1 B, asterisk), suggesting another very minor cleavage site. These results indicate that the C-terminal region extending from Glu217 acts as the primary domain linker that is accessible to trypsin. Based on these data and our findings from this study, we define this ~220-residue-long N-terminal region as a single domain module named "SYLF" domain on the basis of its representative members (SH3YL1, Ysc84p/Lsb4p, Lsb3p, and plant FYVE protein; Fig. S1 B).

The yeast SYLF protein Ysc84p/Lsb4p localizes to actin patches and plays an important role in endocytosis (Dewar et al., 2002). The conserved N-terminal region binds to and forms a bundle of F-actin in vitro (Robertson et al., 2009). We attempted to recapitulate this finding by using SH3YL1, but neither full-length SH3YL1 nor its SYLF domain bound to F-actin (Fig. S1 C). In contrast, the SYLF domains of the budding yeast proteins Ysc84p/Lsb4p and Lsb3p, as well as actinin-1 (ACTN1), which was used as a positive control, showed efficient F-actin binding (Fig. S1 C).

The failure of SH3YL1 to bind F-actin suggests that it is not an evolutionarily conserved biochemical property, at least in mammalian SYLF domains. In addition, in pull-down experiments using HeLa cell lysate and rat brain cytosolic fractions, no proteins bound to the SH3YL1 SYLF domain–GST fusion protein (unpublished data). These results prompted us to examine whether it binds to phospholipids like the BAR and F-BAR domains in the proteins containing C-terminal SH3 domains. As expected, full-length and truncated recombinant proteins containing the SH3YL1 SYLF domain bound well to liposomes that were composed of acidic phospholipids from brain extracts (brain liposomes; Fig. 1 C). In contrast, a deletion mutant that lacked the SYLF domain (ΔSYLF) had nearly no affinity for liposomes. These results demonstrate that the SYLF domain is essential and adequate for lipid binding. Moreover, yeast SYLF domains had high affinities for liposomes (Fig. 1 D), indicating that lipid binding is an evolutionarily conserved property of the eukaryotic SYLF domains.

Next, we assessed the lipid-binding specificity of the full-length protein and found that it bound to $PI(3,4,5)P_3$ with the highest affinity (Fig. 1 E). Other D5-phosphorylated phosphoinositides such as $PI(3,5)P_2$ and $PI(4,5)P_2$ were also preferred compared with other acidic phospholipids. Similar results were obtained with the SYLF domain–only construct (Fig. S2 A), confirming that this module binds to phosphoinositides.

An amphipathic α helix at the N terminus of the SYLF domain is necessary for lipid binding

We observed that the predicted α-helical sequence at the N terminus of the SYLF domain (residues 9–23) contained many

Published May 30, 2011

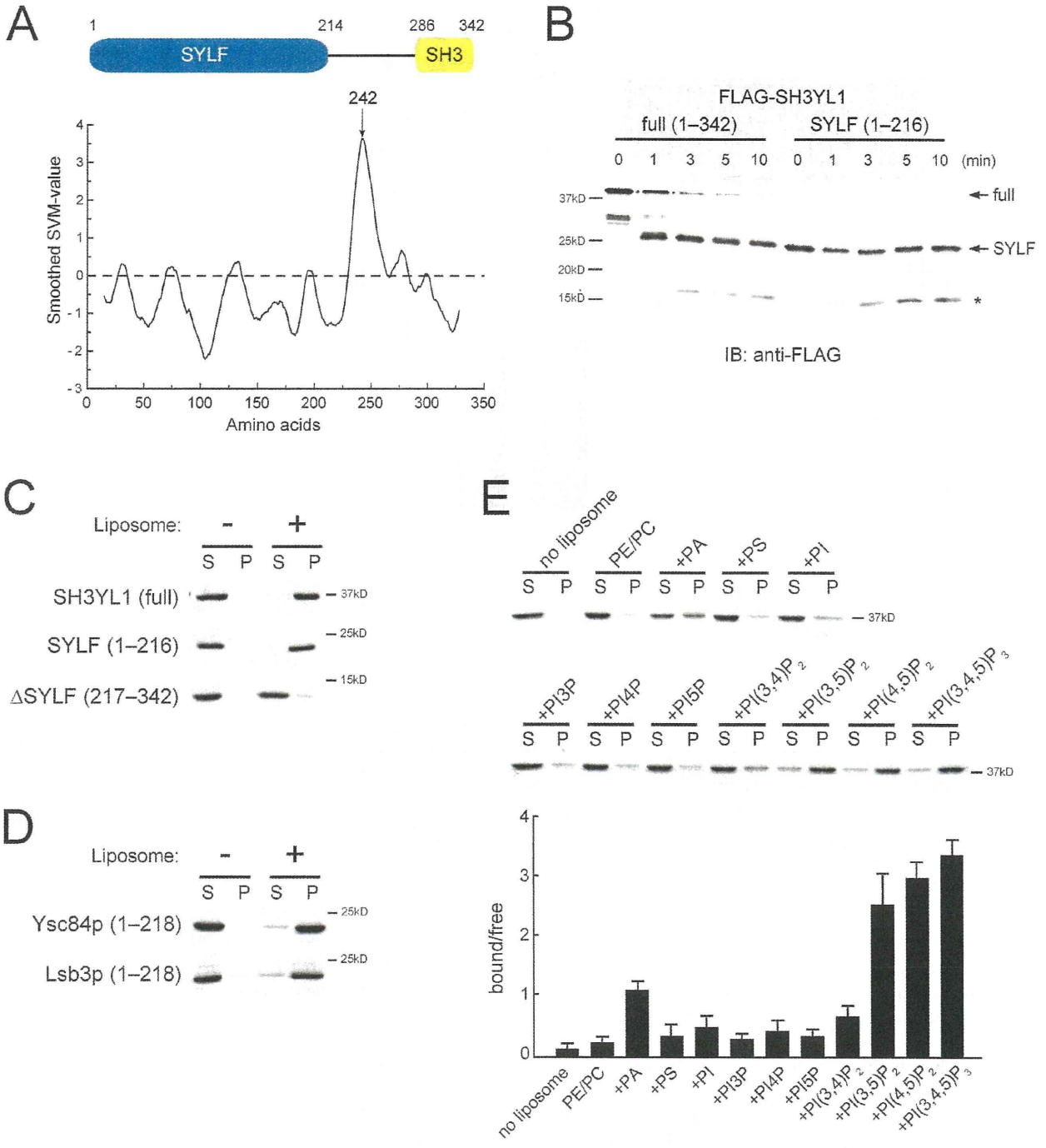

Figure 1. **The N-terminal region of SH3YL1 with high affinity for phosphoinositides.** (A) A schematic presentation of human SH3YL1 and domain linker prediction by the SVM long protocol. Smoothed SVM output values were plotted against the amino acid sequence. Larger values indicate higher probabilities of domain linkers. (B) Limiting proteolytic digestion. Purified FLAG-SH3YL1 (full length and SYLF) proteins were treated with trypsin for the indicated times and then immunoblotted (IB) with anti-FLAG antibodies. The asterisk shows a minor digestion product. (C) Liposome cosedimentation assay using brain liposomes and SH3YL1 (full length, SYLF, and ΔSYLF). Proteins in the supernatant (S) and pellet (P) are visualized by CBB staining. (D) Liposome cosedimentation assay using brain liposomes and Ysc84p and Lsb3p (1–218). (E) PE/PC-based liposomes supplemented with 10% of the indicated lipids were used in the cosedimentation assay and quantitative representation. Results are a mean (SD) of three independent experiments.

positively charged residues (Fig. 2 A). Moreover, this region was predicted to possess amphipathic properties (Fig. 2 B), suggesting that it plays an important role in lipid binding. To test this hypothesis, a deletion mutant (Δ1–29) was constructed and subjected to lipid-binding assay. The deletion mutant (Δ1–29) showed much lower affinity than the full-length protein (Fig. 2 C), indicating the importance of this region. The contribution of the positively charged residues on the hydrophilic surface of

Published May 30, 2011

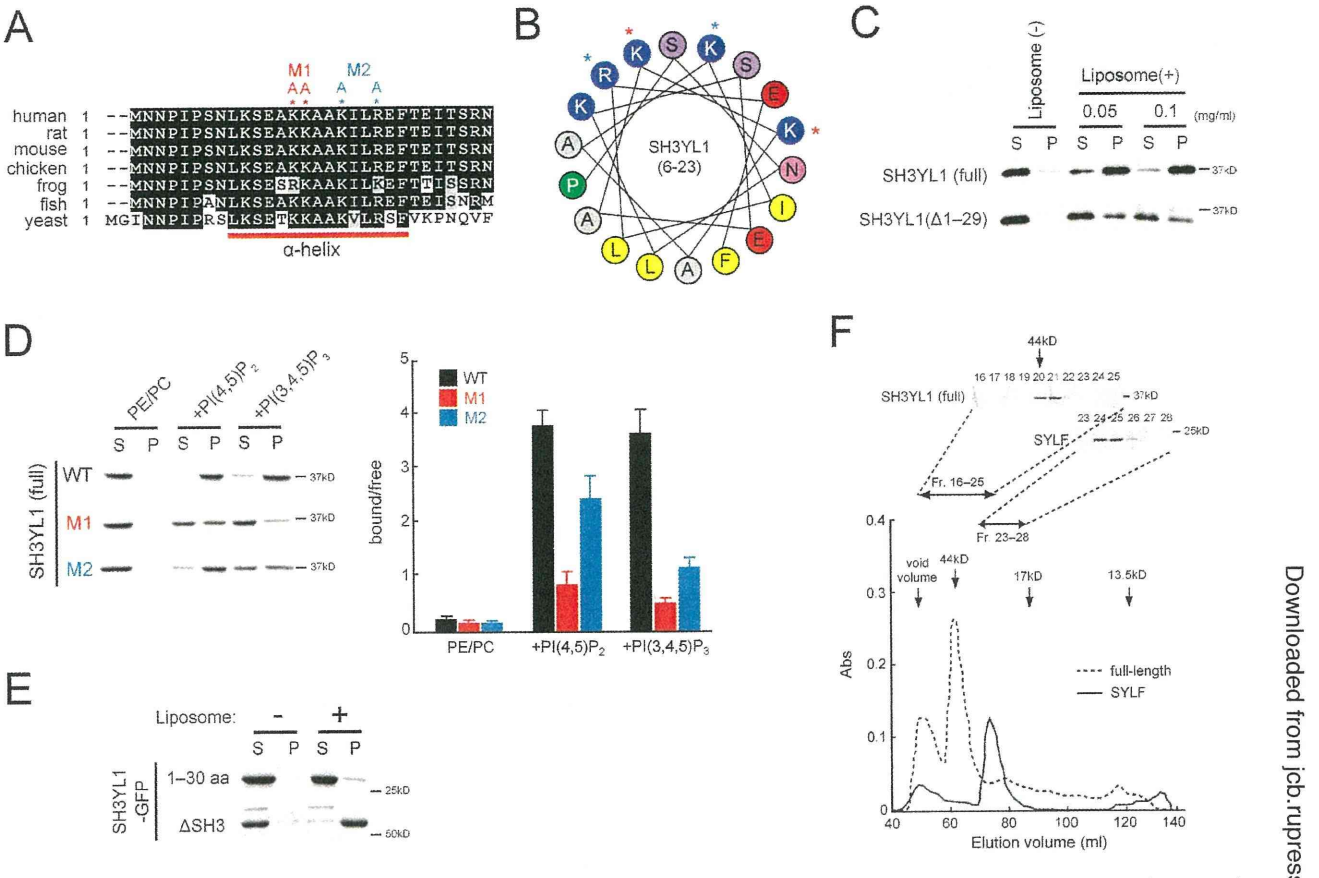

Figure 2. **An amphipathic α helix at the N terminus of the SYLF domain is necessary for lipid binding.** (A) Multiple sequence alignment of N-terminal regions of the SYLF domain from various species. The predicted α helix is indicated by a red line (residues 9–23), and mutated, positively charged residues in M1 and M2 are shown by asterisks. Identical amino acids are shaded in black, and similar residues are in gray. (B) A helical wheel representation of the SH3YL1 N-terminal region. Yellow, hydrophobic residues; purple, serine; blue, basic; pink, asparagine; red, glutamic acid; green, proline; and gray, other residues. Mutated residues are shown by asterisks. (C) Liposome cosedimentation assay using full-length or Δ1–29 SH3YL1 mutant and brain liposomes. Proteins are visualized by immunoblotting with anti-SH3YL1 antibodies. (D) PE/PC-based liposomes supplemented with 10% of $PI(4,5)P_2$ or $PI(3,4,5)P_3$ were used in the cosedimentation assay and quantitative representation. WT, wild type. Results are a mean (SD) of three independent experiments. (E) Liposome cosedimentation assay using 1–30 or ΔSH3 SH3YL1-GFP mutant and brain liposomes. Proteins are visualized by CBB staining. (F) Gel filtration chromatography of SH3YL1 (full length and SYLF). Eluted fractions were measured at 280 nm and then visualized by CBB staining. Abs, absorbance.

this region (Lys14 + Lys15 [M1] or Lys18 + Arg21 [M2]) was determined by replacing them with alanine (Fig. 2, A and B). In comparison with wild type, the binding affinity of these mutants for $PI(3,4,5)P_3$, especially that of the M1 mutant, was significantly low (Fig. 2 D).

Notably, the 30 residues of the N terminus (1–30) bound poorly to the brain liposomes (Fig. 2 E), indicating that this α helix alone is inadequate for binding and that the remainder of the region makes a significant contribution to the lipid binding. This phenomenon was not attributed to the avidity generated as a result of apparent dimerization or oligomerization through the remainder of the region because the full-length SH3YL1 and SYLF domain are monomeric, as shown by gel filtration (Fig. 2 F). Together with the fact that the Δ1–29 mutant still retains ~40% of binding (Fig. 2 C), these data collectively suggest that the SYLF domain has a lipid-binding surface, which is formed by positively charged residues in the N-terminal amphipathic helix and unidentified residues in the remainder of the domain.

SH3YL1 localizes to the plasma membrane at an early stage of dorsal ruffle formation

Growth factor stimulation induces the dynamic and transient formation of membrane ruffles on the dorsal surface of NIH3T3 cells (Mellström et al., 1988; Buccione et al., 2004). Because SH3YL1 strongly bound to $PI(3,4,5)P_3$, which is produced by growth factor stimulation, we investigated whether SH3YL1 localizes to the PDGF-induced dorsal ruffles.

Under serum-starved conditions (0 min), HA-tagged SH3YL1 (HA-SH3YL1) was localized to the cytosol in NIH3T3 cells. 2 min after PDGF stimulation, HA-SH3YL1 was recruited to a plasma membrane structure with short actin filaments that were aligned in a circular pattern (Fig. 3 A). This structure appeared to be an immature form of dorsal ruffles, suggesting that SH3YL1 functions at an early stage of dorsal ruffle formation. At 5 min, HA-SH3YL1 accumulated at mature and circular dorsal ruffles that were rich in dense F-actin structures. Consistent with the observations in previous studies (Araki et al., 1996; Suetsugu et al., 2003), dorsal ruffle formation was

Published May 30, 2011

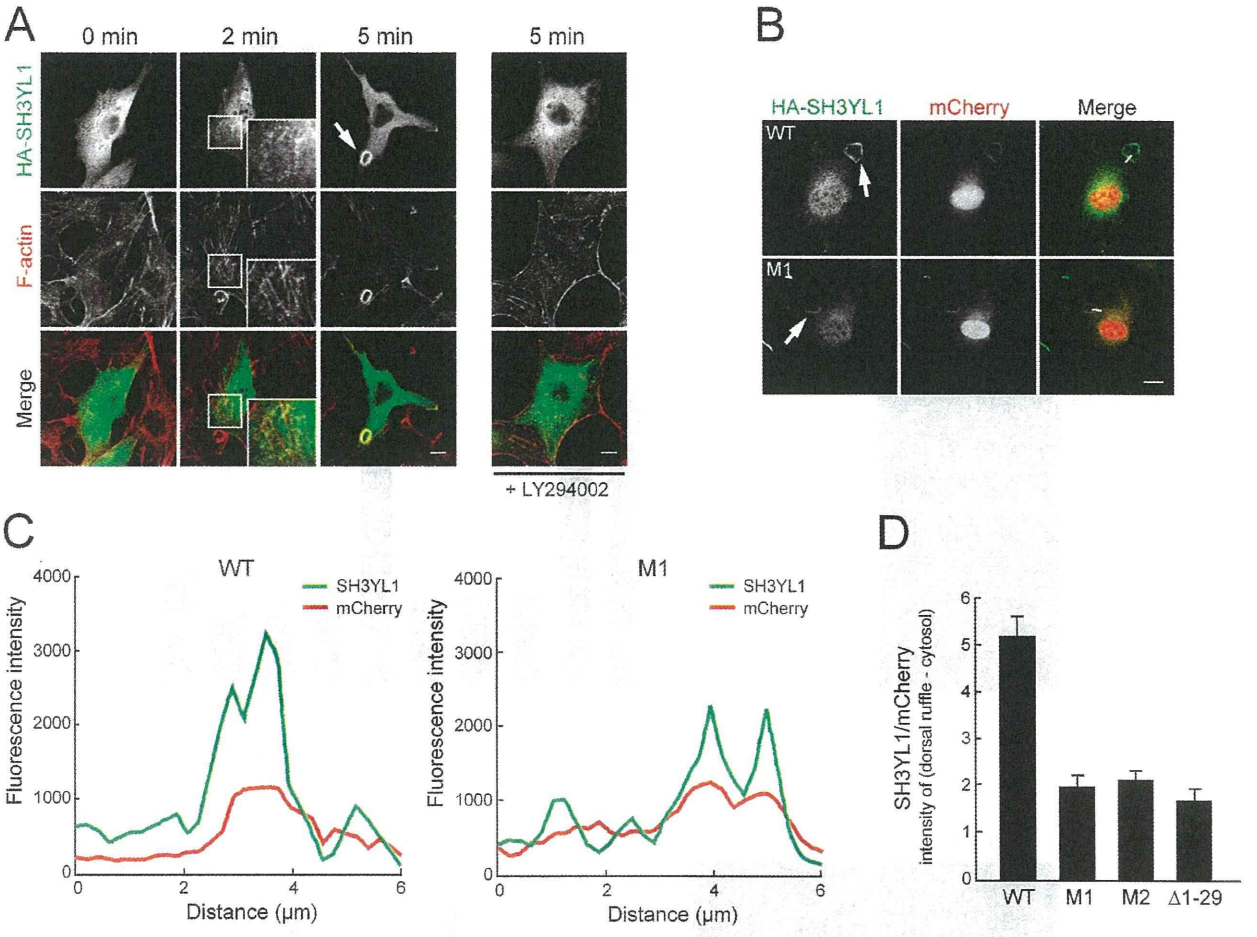

Figure 3. **Localization of SH3YL1 at the dorsal ruffle.** (A) NIH3T3 cells expressing HA-SH3YL1 (full length) were stimulated with 20 ng/ml PDGF for the indicated times and stained with anti-HA antibodies and rhodamine-phalloidin. Insets, precursor structures at a high magnification. Where indicated, 25 μM LY294002 was applied for 30 min before stimulation. (B) Localization of wild-type (WT) HA-SH3YL1 and mutant (M1) at 5 min after PDGF stimulation. (A and B) Arrows, circular dorsal ruffles. Bars, 10 μm. (C) Fluorescence intensity profiles of white lines in B. (D) Fluorescence intensities in the cytosol were subtracted from those at circular dorsal ruffles. The ratio of anti-HA versus mCherry are presented. Results are a mean (SD) of four experiments.

blocked by LY294002, a PI3K inhibitor (Fig. 3 A), indicating that D3-phosphorylated phosphoinositides and their binding partners are involved in this process.

Next, we studied whether the lipid-binding activity of SH3YL1 is required for its localization to the dorsal ruffles. The SYLF domain, which was determined to be essential for phosphoinositide binding, was sufficient for localization to the dorsal ruffles (Fig. S2 B). In addition, the density of the mutant form of SH3YL1, which has reduced affinity for phosphoinositides (Fig. 2 D, HA-SH3YL1 [M1]), was lower at the dorsal ruffles (Fig. 3, B and C) compared with that of the wild type. To quantify these findings, we measured the fluorescence intensities of HA-SH3YL1 as well as mCherry protein, which was coexpressed as a cytosolic marker of the dorsal ruffle area, to calculate the net intensity by subtracting the cytosolic signal. As shown in Fig. 3 D, the localization of the M1, M2, and Δ1–29 mutants to the dorsal ruffles was significantly lower than that observed in the case of wild type, demonstrating that SH3YL1 is recruited to the plasma membrane via PI3K-dependent SYLF–phosphoinositide interactions.

SH3YL1 is necessary for dorsal ruffle formation

Because SH3YL1 localized to the dorsal ruffles, we assessed whether it was necessary for the formation of dorsal ruffles. Transfection of SH3YL1-targeting siRNAs resulted in the depletion of >90% of SH3YL1 protein but did not alter actin levels (Fig. 4 A). Dorsal ruffles were formed in ~60% of control siRNA–treated cells after PDGF stimulation, whereas significantly fewer ruffles were formed in SH3YL1 siRNA–treated cells (Fig. 4, B and C). This suppression was alleviated by the exogenous wild-type SH3YL1 but not by ΔSH3, M1, or M2 constructs (Fig. 4 C), suggesting that the presence of both the SH3 domain and a functional SYLF domain is necessary.

Dorsal ruffles have been implicated in macropinocytosis, which can be monitored with markers for fluid-phase endocytosis. Consistent with the dynamic association of SH3YL1 with dorsal ruffles, PDGF-dependent fluid-phase endocytosis was inhibited in SH3YL1 knockdown cells relative to control cells, as observed by dextran internalization assay (Fig. 4 D). To quantify this effect, we measured the uptake of HRP, a